Journal of Polymers and the Environment (2020) 28:2125–2136
https://doi.org/10.1007/s10924-020-01752-5

ORIGINAL PAPER

Toughening Effect of Physically Blended Polyethylene Oxide on Polyglycolic Acid

Ling-Fei Chang[1] · Ying-Guo Zhou[1] · Yang Ning[1] · Jun Zou[1]

Published online: 15 May 2020

Abstract

Polyglycolic acid (PGA), a linear aliphatic polyester with excellent biodegradability and biocompatibility, is widely used as a medical material. However, the inherent brittleness of this material may limit its use in many other industrial applications. This study explored the toughening effect of physically blending PGA with polyethylene oxide (PEO). Standard tensile samples of different PGA/PEO blends were prepared by a torque rheometer and a microinjection molding machine. The thermodynamic properties, mechanical properties, and microstructure of the PGA/PEO samples were investigated by differential scanning calorimetry (DSC), a universal tensile testing machine, a cantilever impact tester, and field emission scanning electron microscopy (FE-SEM). The experiment ultimately found that the addition of 15 wt% PEO greatly improved the toughness of the blended PGA/PEO. A yielding process could be observed in the tensile tests, and the elongation-at-break increased from 3.67% for pure PGA to 54.14% for PGA/PEO 85:15, which shows an increase of 1475.2%. It can be concluded that the addition of PEO is a good way to increase the PGA toughness. The mechanism of PGA toughening by PEO was further analyzed, and the increase in toughness could be attributed to the existence of a continuous PEO phase that facilitated the formation and evolution of cavities between the partially compatible PGA and PEO phases.

Keywords Polyglycolic acid (PGA) · Polyethylene oxide (PEO) · Mechanical properties · Toughening · Compatibility

Introduction

As a kind of new typical aliphatic polyester, polyglycolic acid (PGA) can be fabricated by the polycondensation of glycolic acid (GA), the ring-opening polymerization of glycolide, and the solid-state polycondensation of halogenoacetate [1, 2]. Unlike conventional fossil fuel-based plastics and rubbers, which are often stable and nondegradable [3], PGA can gradually degrade and eventually become water and carbon dioxide after being used for a certain period. The degradation products are harmless to the human body, animals, plants, and the natural environment. Therefore, PGA is currently well-known as a new type of fully biodegradable and excellent biocompatible coal-based polymer and has been widely used in the biomedical field [4–6], including as medical sutures, controlled drug release carriers, fracture fixation structural elements, tissue engineering stents, and suture reinforcement components [7].

However, due to its inherent brittleness and high crystallinity, the use of PGA may still be limited in many other industrial applications. The most direct and effective method to extend its application range is to increase the PGA toughness. Compared with thousands of studies on the modification of other fossil fuel-based polymers [8], increases in PGA toughness have rarely been reported in the open literature. This is possibly partially due to the high raw material cost of the GA monomer, which reduces the optimization opportunities for further PGA application. However, an improvement in performance can undoubtedly promote wider applications, which in turn reduces costs. Determining a method for toughening PGA is hence worthy of investigation because of the academic research value and the application prospects.

A method for toughening PGA can be easily inspired by that of another aliphatic polyester, polylactic acid (PLA), because of their similar molecular structures, as shown in

✉ Ying-Guo Zhou
zhouyingguo@gmail.com

✉ Jun Zou
zj-881996@163.com

[1] School of Materials Science and Engineering, Jiangsu University of Science and Technology, Zhenjiang 212003, People's Republic of China

Fig. 1. Figure 1 shows that the macromolecular compositions of PGA and PLA are almost the same, except that PLA has one more methyl group than PGA. The rigid macromolecular chains cause PLA to be brittle and stiff. Therefore, increasing the PLA toughness was necessary for its application [9].

Compared to PGA, PLA modification has been more widely researched and analyzed in depth. There are many investigations into PLA toughening [10–26], which can be roughly classified into two categories: physical methods and chemical methods. Certain additives, functional groups or other polymers can be incorporated into the PLA matrices by means of compounding, plasticizing or blending, which was reported to improve the PLA toughness to a certain extent [11–24]. The physical method is known to be highly efficient and easy to implement. However, it is possible that the uniformity of the dispersion and/or mixing can influence the modification efficiency and the performance of the final products. The outcome depends on the detailed blending procedures and technological conditions. In contrast, chemical modification can directly change the molecular composition and/or the molecular chain structure using copolymerization and/or cross-linking [25, 26]. This method can offer a more stable performance than the physical methods. However, the technological process of chemical modification is often extremely complex, and the synthesis efficiency may not be high. Furthermore, combining ring-opening polymerization and physical blending was reported to be a revolutionary method to improve the mechanical properties of PLA matrices [27, 28]. However, the combination method is more complex than the single methods alone.

Considering these concerns, the physical blending method was attempted to toughen PGA in this study. Polyethylene oxide (PEO) is a biodegradable polymer and has been widely used in biomedical fields because of its good biocompatibility and extremely low toxicity. PEO was reported to be a suitable candidate for PLA flexibilizers [14]. Blending PGA with PEO was believed to be a possible solution for improving the PGA toughness. In this study, different PEO contents were melt blended with a PGA matrix, and the thermal properties, mechanical performance, and morphological structure between the phases of the PGA/PEO blends were carefully investigated. The toughening mechanism of PGA by blending with PEO is further discussed.

Experimental

Materials

PGA and PEO were obtained from Jin Ju Alloy Co., Ltd. (Zhenjiang, Jiangsu, China) and Sumitomo Co., Ltd. (Japan), respectively. Their melt flow volumes were 12.3 cm^3/10 min (ISO 1133) and 8.9 cm^3/10 min (ISO 1133), respectively. The relative molecular mass of PEO is approximately 1×10^5.

Sample Preparation

A torque rheometer (RM-400B, Hapro) was used to fabricate PGA/PEO blends. PGA and PEO were added to the chamber in a fixed volume with PEO contents of 0.0 wt%, 5.0 wt%, 10.0 wt%, 15.0 wt%, and 20.0 wt%. The rotational speed and the processing temperature were determined to be 60 rpm and 220 °C, respectively. The rotation lasted for 10 min, and then the mixtures were removed from the rheometer. The plots of torque vs. time were obtained, and the results are shown in Fig. 2. The cooled mixtures were cut into pellets and then injected into standard tensile and impact bars using a microinjection molding machine (Baby Plastics Machinery Co. Ltd, Italy). It is well known that injection molding includes many processing parameters that may influence the

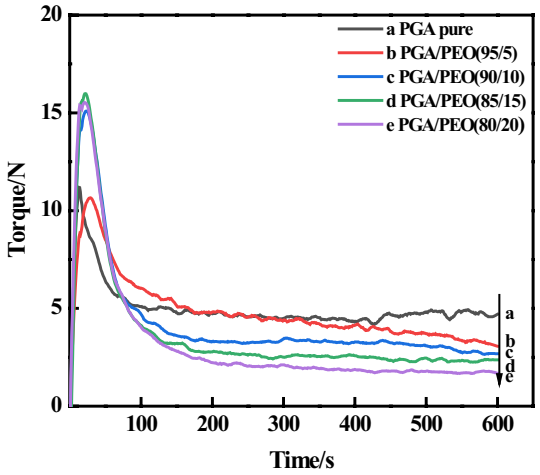

Fig. 2 Plots of torque vs. time of the PGA/PEO blends

Fig. 1 Comparison of the macromolecular structural formulas of PGA and PLA

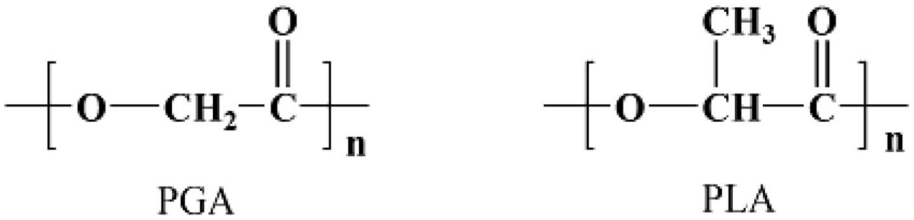

microstructure of the sample, leading to varible mechanical properties. After many screening experiments, the optimal melt temperature, injection pressure, injection time, packing pressure, packing time, and cooling time were set to 240 °C, 50 MPa, 1 s, 40 MPa, 5 s, and 20 s, respectively. All the molded samples were placed at room temperature for 24 hours before the next test and characterization.

Test and Characterization

Fourier transform infrared spectroscopy (FT-IR, FTS2000, Digilab Co. Ltd.) spectra were recorded from 400 to 4000 cm^{-1} with a resolution of 4 cm^{-1} to obtain 64 scans of the PGA/PEO blends.

The thermal behaviors of the PGA/PEO blends were studied by differential scanning calorimetry (DSC, PE, 8000). The specimens with a weight of 4.9 ~ 5.1 mg were sealed in 40 ml aluminum crucibles. Under nitrogen protection, all specimens were cooled to 20 °C, and then heated to 250 °C. After holding at 250 °C for 2 min to eliminate the heat history, the samples were then cooled to 20 °C. The samples were heated to 250 °C once again. All the heating and cooling rates were 10 °C/min for comparison. The cooling and secondary heating curves were recorded.

Tensile testing was performed using a universal testing machine (SANS CMT 4024) equipped with a 10 kN electronic load cell and mechanical grips. The tests were conducted at a crosshead speed of 10 mm/min. All tests were carried out according to the ISO 527 standard and 5 samples were tested for each group to obtain an average value.

The impact test was carried out on an impact tester (UJ-40 cantilever beam) according to the ASTM-D256 standard. Each group of notch samples was tested five times in parallel. The notch was wedge-shaped and the depth was 2 mm.

The morphological structures were examined using field emission scanning electron microscopy (FE-SEM, ZEISS Merlin Compact). It must be noted that the electrons of a common SEM instrument may burn the PGA particles. All specimens were sputter coated with platinum prior to observation. The SEM tests analyzed three parts: the fracture surfaces of the quenched-molded samples, the tensile-tested PGA/PEO 85:15 blend, and the impact-tested PGA/PEO blends. The samples fractured quickly after freezing in liquid nitrogen for 30 min in the quenching procedure.

Results and Discussion

Torque Variation

Figure 2 shows the plot of torque vs. time for the PGA/PEO blends. Figure 2 shows that the equilibrium torque of PGA/PEO decreases with increasing PEO content, indicating that PEO has a plasticizing effect on PGA. The existence of PEO decreases the melt viscosity of PGA/PEO, which may be attributed to the increased space caused by the incorporation of PEO, resulting in a more flexible molecular chain [29]. The decrease in the equilibrium torque also suggests that there is no cross-linking between PEO and PGA during the torque test. Hence, the blending operation can be viewed as a physical processing. This result also suggests that the PGA and PEO phases are not fully compatible, which is an accordance with a recent study of the relationship between compatibility and balance torque [30, 31], since the variation in the balance torque of PGA/PEO blends does not linearly vary with the PEO content.

FTIR

FTIR is well known as a good way to examine the composition of PGA/PEO blends. Figure 3 shows a comparison between the characteristic absorption peaks of pure PGA and the PGA/PEO 85/15 blend. For the PGA/PEO 85/15 blend, the absorption peak at 2888 cm^{-1} shown in Fig. 3a corresponds to a typical $–CH_2–$ bond, and this peak is caused by the stretching vibration of the $–CH_2–$ group of PEO. Furthermore, the stretching vibration of the –CH– group of PEO is superimposed with the stretching vibration of the $–CH_2–$ group, leading to multiple peaks from 1197 to 1505 cm^{-1} (Fig. 3b). The absorption peaks appearing at 1466 cm^{-1}, 1361 cm^{-1}, and 1342 cm^{-1} completely coincide with the multiple peak characteristics in the FTIR diagram of the standard PEO [32]. The peak positions of the PGA/PEO 85:15 blend are almost the same as those of pure PGA, indicating that the blending of PEO and PGA using the torque rheometer is a typical physical entanglement process.

Therefore, it can be concluded that no chemical reaction occurs between the PGA and PEO phases according to the above results of torque testing and FTIR. However, the existence of PEO may influence the thermal behavior of PGA, which is discussed in the following sections.

Thermal Analysis

Figure 5 shows the DSC secondary heating curves of the PGA/PEO blends. The melting temperature (T_m) can first be obtained by the values of the absorption peak on the right in Fig. 4. Pure PGA has a T_m of 215.2 °C. With increasing PEO content, the melting peak of the PGA/PEO blends gradually shifts slightly to the left. Typically, when the content of PEO increases to 20 wt%, the T_m of PGA/PEO blends decreases to 212.0 °C. It is expected that a decrease in T_m occurs with the addition of PEO, which can be attributed to the dilution effect [33]. That is, this result is similar to the effect of adding a small amount of low-molecular-weight plasticizer to a polymer. Furthermore, absorption peaks appear on the

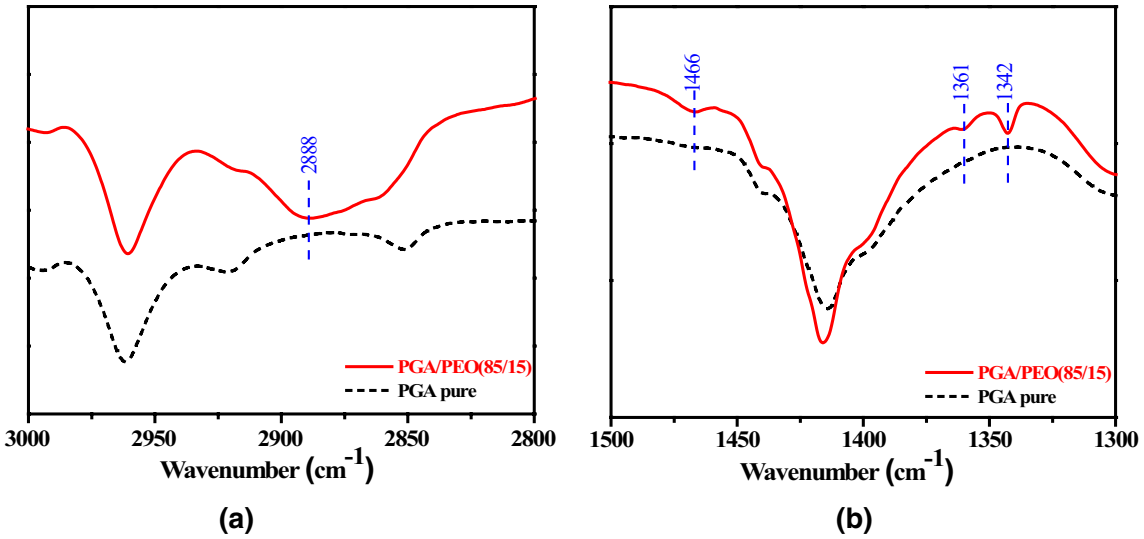

Fig. 3 Comparison between FTIR results of pure PGA and PGA/PEO 85/15 blend

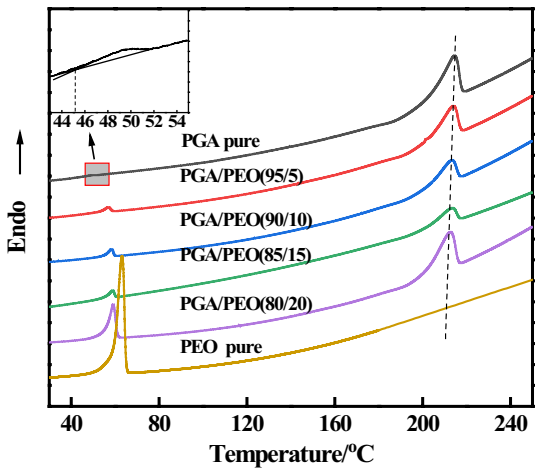

Fig. 4 DSC secondary heating curves of the PGA/PEO blends

Table 1 Thermal performance parameters obtained by DSC curve analysis

Sample	T_g(℃)	T_m(℃)	T_{mc}(℃)	ΔH_m(J/g)	X_c(%)
PGA pure	45.2	215.2	133.4	85.3	44.6
PGA/PEO(95/5)	–	214.3	147.9	52.7	27.6
PGA/PEO(90/10)	–	213.2	149.0	44.6	23.3
PGA/PEO(85/15)	–	212.4	150.2	28.1	14.7
PGA/PEO(80/20)	–	212.0	153.5	58.9	30.8
PEO pure	–	63.0	43.5	184.2	89.1

left in the heating curves of Fig. 4. For pure PGA, the glass transition temperature (T_g) can be determined to be 45.2 °C by the intersection of the tangent of the leading edge of the curve and the baseline, which is shown in the upper left magnified image in Fig. 4. For the PGA/PEO blends, distinct absorption peaks can be observed at approximately 60 °C. It is almost impossible that these absorption peaks come from the T_g of PGA, since PEO cannot improve the T_g of PGA/PEO blends according to fundamental thermodynamic theories. In addition, the peak intensity should not vary with increasing PEO content. To further investigate the attributes of these absorption peaks, a pure PEO heating curve is supplemented and is used as a comparison. Pure PEO has a T_m of 63 °C, which is near the values of the peaks of PGA/PEO blends in Fig. 4. Hence, the absorption peak that appears on the left for the PGA/PEO blends should be the T_m of PEO. Since the PEO in the PGA/PEO blends has undergone mixing at a high temperature and the pure PEO has undergone exactly the opposite, a small amount of thermal degradation results in a decrease in the T_m of the PEO in the PGA/PEO blends. The appearance of two melting peaks for the PGA/PEO blends suggests that the compatibility between the PGA and PEO phases is not very good. This result also indicates that PGA and PEO are generally physically entangled during the mixing process.

In addition to the appearance of a double melting peak, the existence of PEO also affects the intensity of the melting peaks of PGA/PEO blends. The peak intensity is known to be the melting enthalpy (ΔH_m). That is, the ΔH_m of the two components of the PGA/PEO blends varies with increasing PEO content. The ΔH_m is quantitatively calculated according to the DSC test, and the results are listed in Table 1. Table 1 shows that the ΔH_m of the PGA/PEO blends decreases significantly from 85.3 J/g for the PGA/PEO 95:5 blend to 28.1 J/g for the PGA/PEO 85:15 blend with increasing PEO content, indicating that the compatibility of PGA

and PEO improves with increasing PEO content. However, ΔH_m shows an increasing trend when the PEO content increases to 20 wt%. This unexpected increase in ΔH_m shown for the PGA/PEO 80:20 blend can be attributed to the phase separation caused by the excessive PEO addition. It is therefore suggested that the incompatibility between PGA and PEO phases increases at this ratio.The partial compatibility between the PGA and PEO phases at different ratios can be further analyzed by the crystallization behavior, since the secondary heating actually originates from the cooling process. Figure 5 shows the DSC cooling curve of the PGA/PEO blends. From the PGA pure curve shown in Fig. 5, the melting crystallization temperature (T_{mc}) of pure PGA is 133.4 °C. After the addition of 5 wt% PEO, the T_{mc} of the PGA/PEO blend increases significantly to 147.9 °C. With increasing PEO content, the T_{mc} increases continuously and is 153.5 °C for the PGA/PEO 80:20 blend. The increase in T_{mc} indicates that the ability of the PGA molecular segment to move is possibly enhanced due to the existence of PEO, which facilitates PGA crystallization. Compared to the crystallization behavior of PGA, that of PEO seems to be more complex. For comparison, the results of pure PEO are also supplied. As shown in Fig. 5, the T_{mc} of pure PEO is approximately 43 °C. However, almost no crystallization peaks appear for the PGA/PEO blends with PEO contents of 5 wt%~15 wt%. For the PGA/PEO 80/20 blend, a small crystallization peak can be observed in the same position of 43 °C. On the one hand, these results indicate that the existence of PGA and PEO phases influences their crystallization processes. Good compatibility between the PGA and PEO phases means that the two phases may be entangled with each other, which destroys the regularity of the PEO phases; hence, the crystallization peaks of PEO cannot be observed. It is therefore suggested that the compatibility of the two phases is not poor, especially for PGA/PEO blends with PEO contents of 5 wt%~15 wt%. On the other hand, the results also indicate that the two phases of PGA and PEO crystallize separately during the cooling process. In particular, the phase separation between PGA and PEO occurs with the addition of 20 wt% PEO to the PGA matrix, suggesting that the compatibility between the two phases decreases. Therefore, the PGA and PEO phases may be partial compatible, which is consistent with the results from the second heating process. In addition, the crystallinity (X_c) can be calculated by the following expression [26]:

$$X_c = \Delta H / \Delta H_F \times 100\% \quad (1)$$

where ΔH_F is the enthalpy of the fully crystallinity PGA sample. Table 1 shows the X_c of the PGA obtained from the cooling process, which shows a trend similar to that of the melt enthalpy in the second heating process. X_c decreases from 44.6% for pure PGA to 14.7% for PGA/PEO 85:15. The

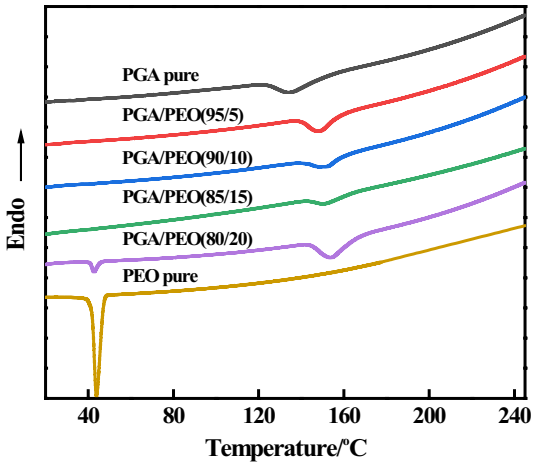

Fig. 5 DSC cooling curves of the PGA/PEO blends

decreasing trend does not continue with a further increase in PEO content. Instead, X_c increases to 30.8% when the PEO content is 20 wt%. The influence of the PEO content on the X_c of the PGA/PEO blend can be attributed to the difference in the partial compatibility between the PGA and PEO phases caused by the PEO content. Good compatibility between the PGA and PEO phases destroys the regularity of PGA phases, and hence, the X_c of PGA decreases and vice versa.

In addition, it is well known that X_c influences and even determines the mechanical properties of a semicrystalline polymer [34–36]. Generally, a decrease in X_c may lead to reduced strengths and moduli and improved toughness and flexibility. It is therefore necessary to investigate the mechanical properties of PGA/PEO blends, which are discussed as follows.

Mechanical Properties

Figure 6 shows the representative stress-strain plots of the PGA/PEO blends, and Fig. 7 shows the results for tensile strength and elongation-at-break. As shown in Fig. 6, the incorporation of PEO results in significant variation in the toughness of the PGA/PEO blends. The elongation-at-break of pure PGA is only 3.67%, indicating that PGA has obvious brittle fracture characteristics. With the addition of PEO, the PGA/PEO blends (Fig. 6b, c, d, and e) show obvious yielding processes in the tensile tests, indicating that the brittle fracture has gradually changed to ductile fracture. The toughness also significantly increases, as evidenced by the elongation-at-break of 13.66% and 39.96% for the PGA/PEO 95:5 and PGA/PEO 90:10 blends, respectively. Moreover, the elongation-at-break can further increase to 54.14% for the PGA/PEO 85:15 blend, which is 1475.2% higher than that of pure PGA. Unfortunately, the tensile strength of the

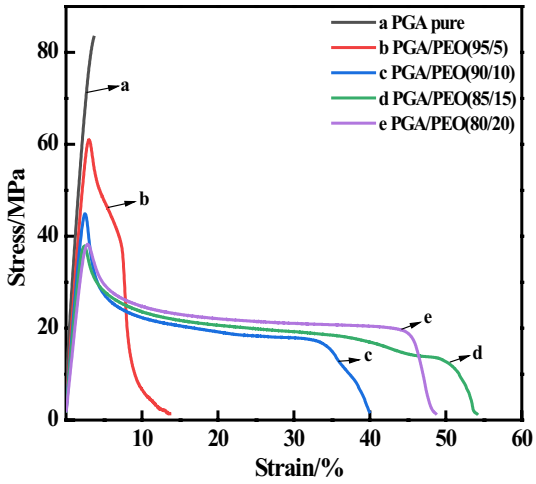

Fig. 6 Representative plots of stress vs. strain of the PGA/PEO blends. Curves of tensile strength and elongation of different PGA/PEO blend contents

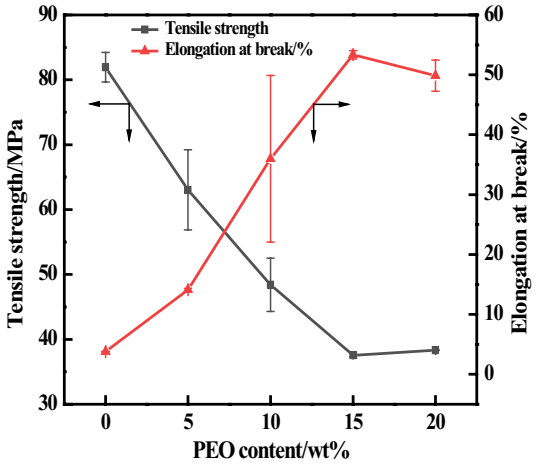

Fig. 7 Results of tensile strength and elongation-at-break for the PGA/PEO blends

PEO/PGA blends decreases significantly from 83.32 MPa for pure PGA to 37.85 MPa for the PGA/PEO 85:15 blend, indicating that the rigidity of PGA decreases as the toughness increases. The reported tensile strengths are nominal values, i.e., the maximum load divided by the original cross-sectional area of the tested samples. It is expected that the strengthening or toughening technologies possibly account for these results, similar to the results of many other modifications of mechanical properties [37–43]. It can also be observed from Figs. 6 and 7 that the addition of 20 wt% PEO results in a slight increase in tensile strength and a decrease in elongation-at-break. This trend is in good agreement with the variation of X_c obtained from the abovementioned DSC analysis. This result is possibly due to a weakening of the mechanical properties caused by the excessive PEO addition in the partially compatible PGA matrix. This idea can be further verified by the SEM results presented in the next section.

To further investigate the effect of PEO on the toughness of PGA/PEO blends, the notched impact strength of the different PGA/PEO blends is also determined. Figure 8 shows the results of the impact strength of the PGA/PEO blends, revealing that the impact strength of the PGA/PEO blends is significantly higher than that of pure PGA. This parameter increases from 26.15 kJ/m^2 of pure PGA to 36.87 kJ/m^2 for the PGA/PEO 85:15 blend, which coincides with the fact that the tensile strength decreases while the impact strength increases in the toughening system.

Morphological Structure

To further study the toughening effect and toughening mechanism of the PGA/PEO blends, the morphological structure of the PGA/PEO blends was explored using SEM characterization. Figure 9 shows the SEM images of the quenched section of PGA/PEO blends. It can be observed from the quenched section of the pure PGA shown in Fig. 9a that the surface of pure PGA is smooth, indicating that it is brittle and rigid. However, when 5 wt% PEO is added to the PGA matrix (Fig. 9b), the fracture surfaces of the PGA/PEO blends are slightly wrinkled. This means that the PGA/PEO 95:5 blend cannot yet be fractured smoothly even in the low-temperature environment of liquid nitrogen quenching, indicating that the addition of a small amount of PEO has already produced a toughening effect on the PGA/PEO blend. With increasing PEO content (Fig. 9c and d), the quenched PGA/PEO blends become increasingly rough, and the wrinkling phenomenon is more easily observed. Hence,

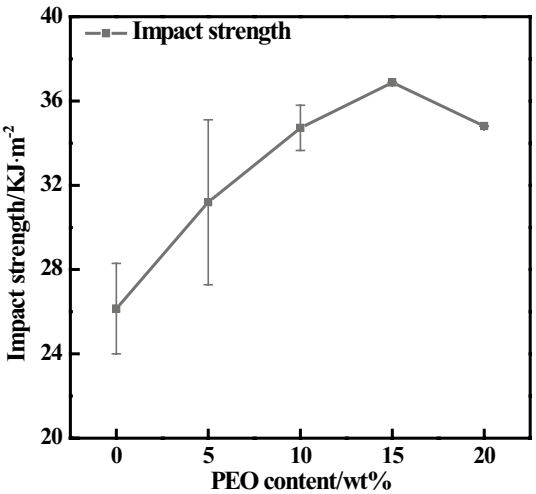

Fig. 8 Results of impact strength for the PGA/PEO blends

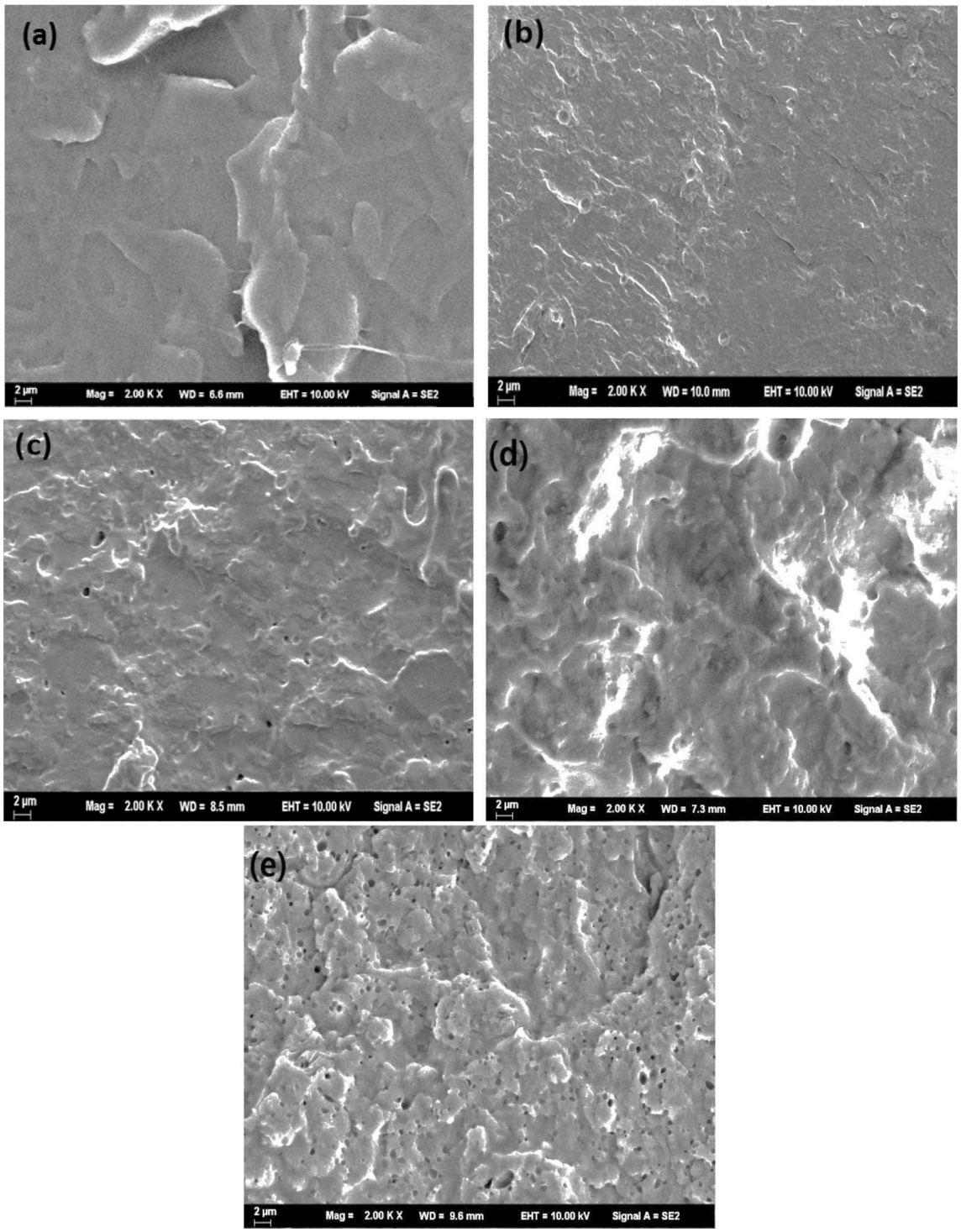

Fig. 9 SEM images of the quenched section for the PGA/PEO blends: **a** pure PGA, **b** 5 wt% PEO, **c** 10 wt% PEO, **d** 15 wt% PEO and **e** 20 wt% PEO

the toughness effects are more remarkable as the PEO content increases. This result is in good agreement with the test results of the mechanical properties presented in Fig. 6 and Fig. 7. Furthermore, the PEO phases can be distributed uniformly into the PGA matrix (Fig. 9b ~ d), indicating that the compatibility between the PEO and PGA phases at this composition is relatively good. However, when 20 wt% PEO is added to the PGA matrix (Fig. 9e), the wrinkling

phenomenon described before is significantly weakened, and the surface begins to become smooth. In particular, many fine voids can be found in Fig. 9e, indicating that the compatibility between the two phases decreases at this composition of PEO and PGA, resulting in the aggregated PEO particles being peeled off from the PGA matrix by external force under quenching. The results of the morphological observations by SEM characterization are also therefore consistent with the previous analysis of compatibility between the two phases.

Classical percolation theory can explain how the dispersion of PEO in the PGA matrix improves the toughness of PGA/PEO [44, 45], as shown in Fig. 10, which has also often been used to analyze the toughening mechanism of many polymer composites [46–50]. When 5 wt% PEO is added to PGA (Fig. 10a), the PEO randomly disperses in the matrix. However, the relatively small amounts of the PEO phase cannot correlate with each other, and the PGA/PEO blend still shows brittle fracture in the tensile test. As the PEO content increases to 10 wt% (Fig. 10b), an association occurs between the PEO phases, and the percolation threshold is almost reached. A percolation channel appears in the PGA matrix, and the PGA/PEO blend can transform from brittle to ductile fracture. When the PEO content is further increased to 15 wt% (Fig. 10c), the PEO and PGA gradually form a cocontinuous sea-island structure, and the toughness of PGA is greatly improved. However, the PEO content continues to increase, leading to obvious phase separation caused by the partial compatibility between the PGA and PEO phases. As a result, the toughness of the PEO/PGA 80:20 blend decreases, as shown in Figs. 6 and 7.

The above results can also be further confirmed by the morphological characterization of the tested impact fracture surfaces of PGA/PEO blends, which are shown in Fig. 11. Figure 11a shows that the surface of pure PGA is almost completely smooth and exhibits typical characteristics of brittle fracture, although it is slightly tougher than the fracture surface frozen by liquid nitrogen (Fig. 9a). Therefore, it is expected that the notched impact strength of pure PGA is generally low, as evidenced by the results shown in Fig. 8. Compared with those of pure PGA, the SEM results of the PGA/PEO blends (Fig. 11b ~ e) show obviously rough surfaces. This can be attributed to the fracture toughness during the impact test. Furthermore, the brittle ductile transition and the increase in the impact strength are gradual. When 5 wt% PEO is added into the PGA matrix (Fig. 11b), the surface of the section is somewhat rougher than that of pure PGA, and slightly more cavities can be observed. When the PEO content increases to 10 wt% and 15 wt% (Fig. 11c, d), the section of the PGA/PEO blends is largely covered with dense cavities, and the PEO is dispersed in the PGA to form a good cocontinuous structure. The PEO particles dispersed in the PGA matrix can act as stress-release agents, which can induce many cavities [51, 52], thereby absorbing a large amount of impact energy. Additionally, due to the mutual interference of the stress fields between the cavities, most of the cavities are terminated by other cavities, which limits the fracture of cavities between adjacent two particles. The termination of cavities greatly improves the toughness of the material. It must be noted that there must be a certain degree of compatibility between the two phases in the blend. Two fully compatible phases can act as one phase, meaning cavities cannot form. However, an extreme incompatibility means that the interface force of the two phases worsens, leading to macroscopic phase separation, as shown in the deformation of the PGA/PEO 80:20 blend. When the PEO content is further increased to 20 wt% (Fig. 11e), interfacial peeling occurs, resulting in the early formation of cracks, which also suggests that the excessive addition of PEO causes separation of the two phases. Therefore, the impact strength of the PGA/PEO blends of 20 wt% PEO instead shows a downward trend. These features are similar to those of the quenched sections of the PGA/PEO blends shown in Fig. 9b ~ e, indicating that the existence of PEO helps the PGA/PEO blends to improve the plastic deformation ability because of the formation of cavities. The plastic deformation

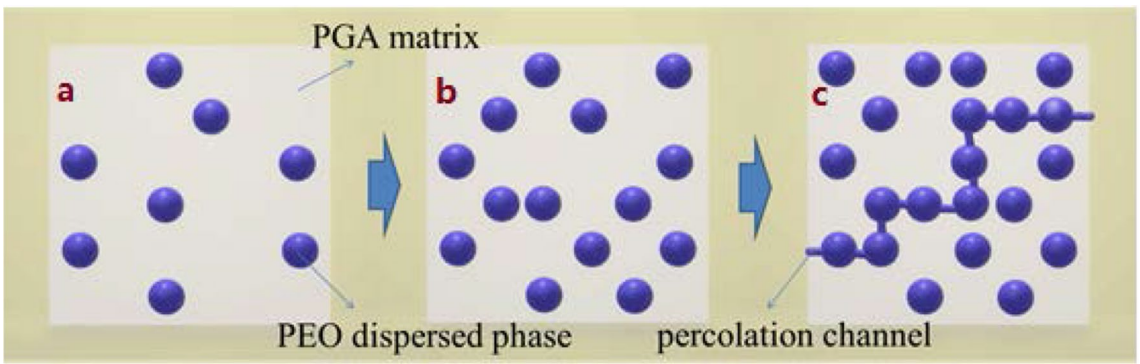

Fig. 10 Model interpretation of the formation of the continuous PEO phase based on percolation theory

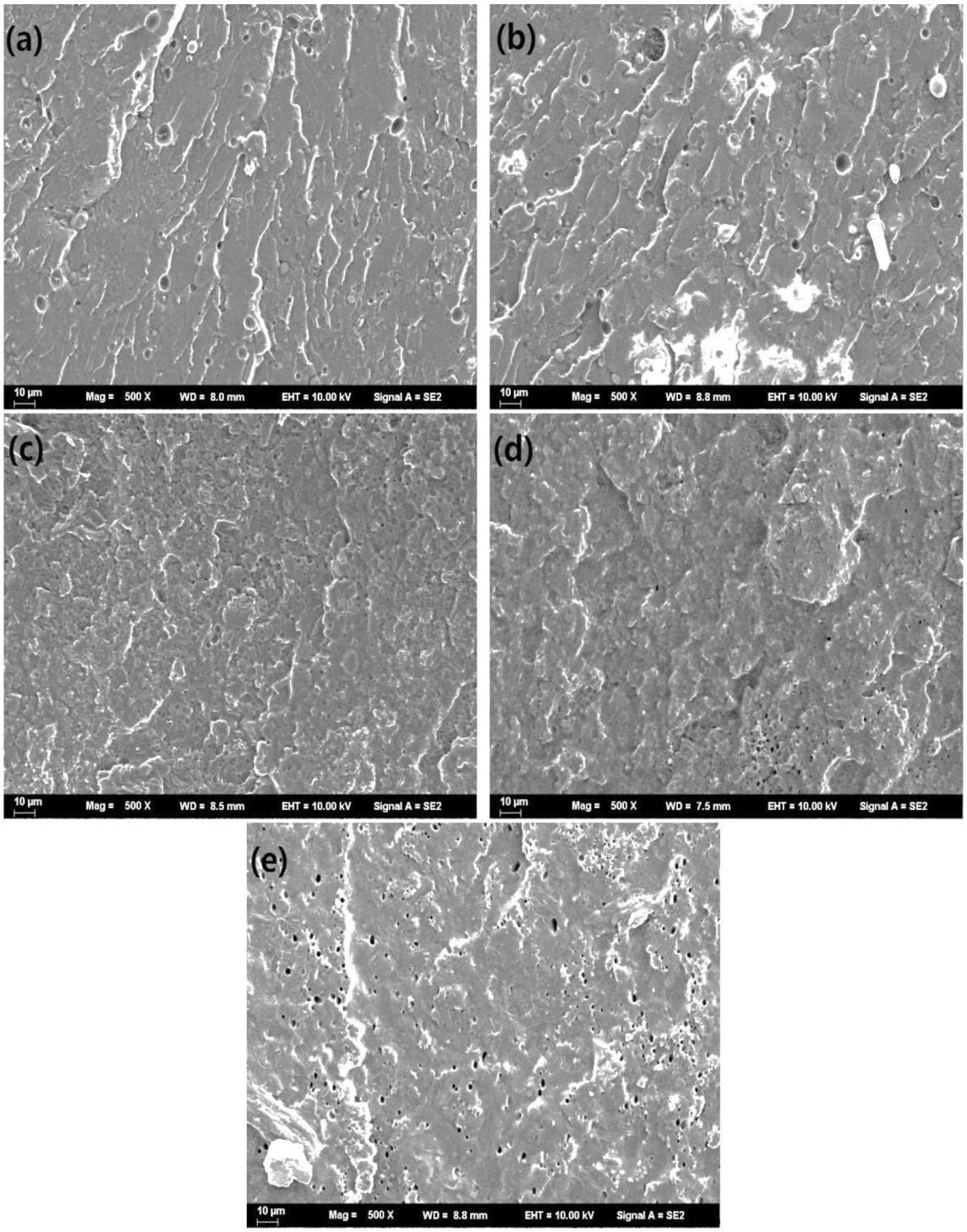

Fig. 11 SEM images of the impact fracture surfaces of the PGA/PEO blends: **a** pure PGA, **b** 5 wt% PEO, **c** 10 wt% PEO, **d** 15 wt% PEO and **e** 20 wt% PEO

ability can effectively disperse the impact energy and hence gradually improve the impact strength of the PGA/PEO blends with increasing PEO content. Because PGA and PEO are not fully compatible, PEO leads to phase separation and induces the generation of cracks. The effects of cracks and cavities are opposite. Cracks cannot absorb more energy but greatly reduce the toughness of materials.

To further verify the toughening mechanism of PGA toughened by PEO, the tensile-test sample of the PGA/PEO 85:15 blend was selected for morphological observation.

Figure 12 shows the three representative characteristic quenched regions, the unstretched (Fig. 12a), transition (Fig. 12b), and necking (Fig. 12c) regions. Figure 12 shows the effect of PEO on the deformation of PGA/PEO during the tensile test. In the unstretched region, there are some scattered voids caused by the PEO phases in the quenching process, which are difficult to observe from the SEM image in Fig. 12a. However, the voids in the transition region become more obvious and larger than those in the unstretched region, as shown in Fig. 12b, indicating the fibrillization of the PEO phases in the tensile test. This can be explained as follows. As a toughening phase, PEO is known to have a higher Poisson's ratio than pure PGA. When PGA/PEO is subjected to an external tensile force, the percolation channel made up of PEO particles acts as continuous stress-released PEO phases, leading to deformation and three-dimensional stress at the edge of the PEO phase. Since the PEO and PGA phases are partially compatible, when the material is stretched, cavities are formed between the PEO and PGA partially compatible interfaces, similar to the impact process mentioned before. The many cavities formed in the tensile process can release the tensile stress and cause variation in the three-dimensional stress field in the surrounding PGA matrix. As a result, the PGA matrix is more prone to yielding, absorbing more energy, and exhibiting ductile fracture. As the force further increases, the PEO phase can be stretched to the shape of an ellipsoid and even other irregular shapes. Since the sample is obtained perpendicular to the direction of stretching (Fig. 12b) and the ellipsoidal-type voids are cut off in the middle, deformed voids can be observed. Therefore, the partially compatible feature of the PGA/PEO phases facilitates an increase in toughness of the PGA/PEO blends. Moreover, the continuous PEO phases can be further drawn into filament shapes under necking, and many irregular voids can be observed from Fig. 12c. The filament-shaped PEO phases can be drawn continuously until cracking and fracture of the PEO phases occur. In conclusion, there are two important factors in increasing the toughness of PGA/PEO blends, the formation of continuous PEO phases and the proper compatibility between the PGA and PEO phases, and both are facilitated by the formation and evolution of cavities between the two phases.

The increase in the toughness of PGA/PEO blends can be attributed to the formation and evolution of continuous PEO phases in the PGA/PEO blends with proper compatibility, which can be attributed to the existence of a continuous PEO phase facilitating the formation and evolution of cavities between the partially compatible PGA and PEO phases.

Conclusions

In this study, PGA/PEO blends were prepared by adding different contents of PEO to PGA matrices. The experimental results show that as the PEO content increases, the equilibrium torque of the PGA/PEO blends shows a downward trend, which is due to the lubricating effect of PEO. The torque of the PGA/PEO blends does not show a slope or an upward trend, indicating that no cross-linking occurs between PEO and PGA. FTIR analysis also indirectly indicates that PEO has a toughening effect on PGA by means of

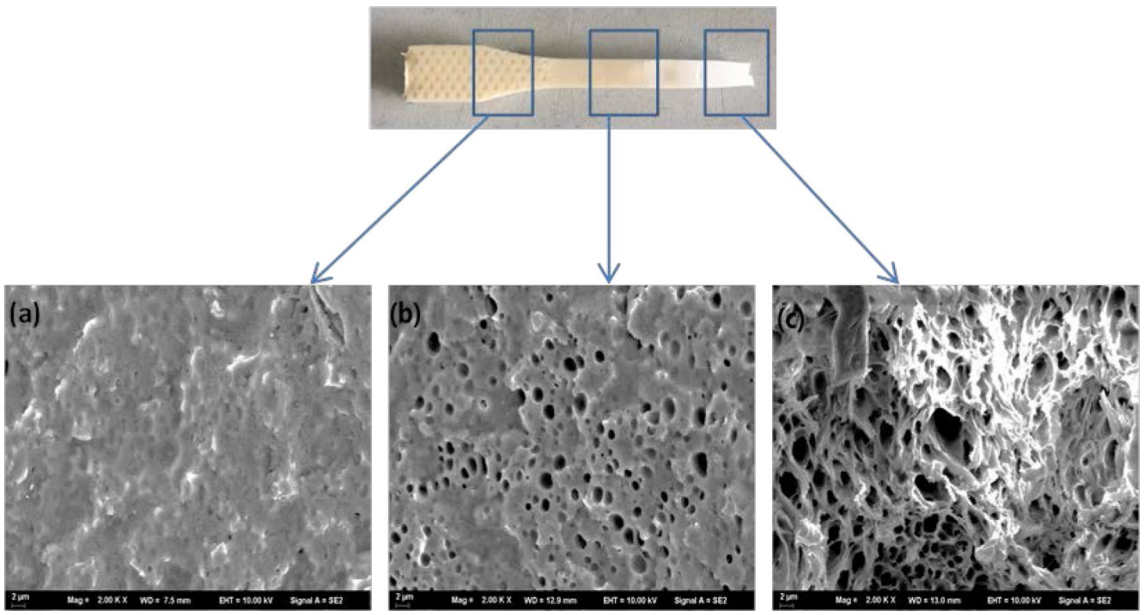

Fig. 12 SEM images of tensile tested sample of PGA/PEO 85/15 blend: **a** unstretched region, **b** transition region, and **c** necking region

physical entanglement. DSC analysis shows that the addition of PEO produces a dilution effect, and the thermal behaviors between the PGA and PEO phases are mutually influential, indicating that the two phases are partially compatible and that excessive addition of PEO can cause macroscale phase separation. This conclusion is further proven by the following tensile tests, impact tests, and SEM characterization. The tensile and impact tests show that the PGA/PEO blends with 15 wt% PEO obtain the best toughness, as evidenced by the elongation-at-break increase of 1475.2% compared with that of pure PGA, with a value from 3.67% for pure PGA to 54.14% for the PGA/PEO 85:15 blend. The impact strength of the PGA/POE blend is also significantly higher than that of pure PGA, increasing from 26.15 kJ/m^2 to 36.87 kJ/m^2. It can therefore be concluded that the addition of PEO is a good way to increase the PGA toughness. It can be further concluded that the evolution of the cocontinuous structure in the partially compatible blends is the main reason for increasing the toughness of PGA/PEO blends, since this evolution facilitates the formation of cavities during deformation.

Acknowledgements The financial support of the Jiangsu Province Industry-University-Research Project (BY2018180) and the Open Project Fund for Jiangsu Provincial Engineering Laboratory for Advanced Materials of Salt Chemical Industry (SF201604) are gratefully acknowledged.

Data Availability All data included in this study are available upon request by contact with the corresponding author.

Compliance with Ethical Standards

Conflict of Interest On behalf of all authors, the corresponding author states that there is no conflict of interest.

References

1. Göktürk E, Pemba AG, Miller SA (2015) Polyglycolic acid from the direct polymerization of renewable C1 feedstocks. Polym Chem 6:3918–3925
2. Shi G, Che Y, Zhou Y, Bai X, Ni C (2015) Synthesis of polyglycolic acid grafting from sodium alginate through direct polycondensation and its application as drug carrier. J Mater Sci 50:7835–7841
3. Ammala A, Bateman S, Dean K, Petinakis E, Sangwan P, Wong S, Yuan Q, Yu L, Patrick C, Leong KH (2011) An overview of degradable and biodegradable polyolefins. Prog Polym Sci 36:1015–1049
4. Mooney DJ, Mazzoni CL, Breued C, McNamara K (1996) Stabilized polyglycolic acid fibre-based tubes for tissue engineering. Biomaterials 17(2):115–124
5. Athanasiou KA, Niederauer GG, Agrawal CM (1996) Sterilization, toxicity, biocompatibility and clinical applications of polylactic acid/polyglycolic acid copolymers. Biomaterials 17(2):93–102
6. Mikos AG, Bao Y, Cima LG, Ingber DE, Vacanti JP, Langer R (1993) Preparation of poly(glycolic acid) bonded fiber structures for cell attachment and transplantation. J Biomed Mater Res 27(2):183–189
7. Gilding DK, Reed AM (1979) Biodegradable polymers for use in surgery polyglycolic/poly(actic acid) homo- and copolymers: 1. Polymer 20(12):1459–1464
8. Meijer HEH, Govaert LE (2005) Mechanical performance of polymer systems: the relation between structure and properties. Prog Polym Sci 30:915–938
9. Anderson KS, Schreck KM, Hillmyer MA (2008) Toughening polylactide. Polym Rev 48:85–108
10. Farah S, Anderson DG, Langer R (2016) Physical and mechanical properties of PLA, and their functions in widespread applications-A comprehensive review. Adv Drug Deliv Rev 107:367–392
11. Balakrishnan H, Hassan A, Wahit MU (2010) Novel toughened polylactic acid nanocomposite: mechanical, thermal and morphological properties. Mater Des 31:3289–3298
12. Jiang L, Zhang J, Wolcott MP (2007) Comparison of polylactide/nano- sized calcium carbonate and polylactide/montmorillonite composites: reinforcing effects and toughening mechanisms. Polymer 48:7632–7644
13. Jiang L, Wolcott MP, Zhang J (2006) Study of biodegradable polylactide/poly(butylene adipate-co-terephthalate) blends. Biomacromol 7:199–207
14. Nijenhuis AJ, Colstee E, Grijpma DW, Pennings AJ (1996) High molecular weight poly(ethylene oxide) blends: thermal characterization and physical properties. Polymer 37(26):5849–5857
15. Arjmandi R, Hassan A, Eichhorn SJ (2015) Enhanced ductility and tensile properties of hybrid montmorillonite/cellulose nanowhiskers reinforced polylactic acid nanocomposites. J Mater Sci 50:3118–3130
16. Meng B, Tao J, Deng J, Wu Z, Yang M (2011) Toughening of polylactide with higher loading of nano-titania particles coated by poly(ε- caprolactone). Mater Lett 65:729–732
17. Peponi L, Navarro-Baena I, Sonseca A, Gimenez E, Marcos-Fernandez A, Kenny JM (2013) Synthesis and characterization of PCL–PLLA polyurethane with shape memory behavior. Eur Polymer J 49(4):893–903
18. Geyter ND, Morent R, Desmet T (2010) Plasma modification of polylactic acid in a medium pressure DBD. Surf Coat Technol 20(4):3272–3279
19. Bulota M, Hughes M (2012) Toughening mechanisms in poly(lactic) acid reinforced with TEMPO-oxidized cellulose. J Mater Sci 47:5517–5523
20. Taib RM, Ghaleb ZA, Ishak ZAM (2012) Thermal, mechanical, and morphological properties of polylactic acid toughened with an impact modifier. J Appl Polym Sci 123:2715–2725
21. Rashmi BJ, Prashantha K, Lacrampe MF, Krawcza P (2015) Toughening of poly(lactic acid) without sacrificing stiffness and strength by melt-blending with polyamide 11 and selective localization of halloysite nanotubes. eXPRESS Polym Lett 8:721–735
22. Hong H, Wei J, Yuan Y, Chen FP, Wang J (2011) A novel composite coupled hardness with flexibleness-polylactic acid toughen with thermoplastic polyurethane. J Appl Polym Sci 121:855–861
23. Li Y, Shimizu H (2007) Toughening of polylactide by melt blending with a biodegradable poly(ether)urethane elastomer. Macromol Biosci 7:921–928
24. Qu X, Jiang LL, Zhang J, Wolcott MP (2007) Comparison of polylactide/nano-sized calcium carbonate and polylactide/montmorillonite composites: reinforcing effects and toughening mechanisms. Polymer 48:7632–7644
25. Shen J, Jiang W, Liu Y (2014) Synthesis characterization and thermal properties of polystyrene-poly (lacticacid)-polystyrene

triblock copolymer via atom transfer radical polymerization. J Thermoplast Compos Mater 8(27):1074–1084
26. Cohn D, Holvely S (2005) Designing biodegradable multibloek PCL-PLA thermos-plastic elastomers. Biomaterials 26(15):2297–2305
27. Lei XX, Lu H, Lu L, Xu HQ, Zhou YG, Zou J (2019) Improve the thermal and mechanical properties of poly(L-lactide) by forming nanocomposites with an in-situ ring-opening intermediate of poly(L-lactide) and polyhedral oligomeric silsesquioxane. Nanomaterials 9(5):748
28. Liu Z, Hu D, Lin H, Li W, Tian J, Lu L, Zhou CJ (2018) Simultaneous improvement in toughness, strength and biocompatibility of poly(lactic acid) with polyhedral oligomeric silsesquioxane. Chem Eng J 346:649–661
29. Chrissafis K (2009) Kinetics of thermal degradation of polymers. J Therm Anal Calorim 95(1):273–283
30. Su B, Zhou YG, Dong BB, Yan C (2019) Effect of compatibility on the foaming behavior of injection molded polypropylene and polycarbonate blend parts. Polymers 11(2):300
31. Tan XT, Zhou YG, Zhou JJ, Dong BB, Liu CT, Xu BP (2019) Effect of acrylonitrile-butadiene-styrene terpolymer on the foaming behavior of polypropylene. Cell Polym 38(3–4):47–67
32. Dhatarwal P, Sengwa RJ (2019) Polymer compositional ratio-dependent morphology, crystallinity, dielectric dispersion, structural dynamics, and electrical conductivity of PVDF/PEO blend films. Macromol Res 27(10):1009–1023
33. Larsen AL, Sommerlarsen P, Hassager O (2006) Dynamic dilution effects in polymeric networks. e-Polymers 6(1):555–565
34. Zhou YG, Wu WB, Lu GY, Zou J (2017) Isothermal and non-isothermal crystallization kinetics and predictive modeling in the solidification of poly(cyclohexylene dimethylene cyclohexanedicarboxylate) melt. J Elastomers Plast 49(2):132–156
35. Su B, Zhou YG, Wu H (2017) Influence of mechanical properties of PP/LDPE nanocomposites: compatibility and crystallization. Nanomater Nanotechnol 7:1–11
36. Su B, Zhou YG (2019) Improvement of transparencies and mechanical properties of poly(cyclohexylene dimethylene cyclohexanedicarboxylate) parts using a compounding nucleating agent to control crystallization. Materials 12(4):563
37. Zhou YG, Zou JR, Wu HH, Xu BP (2020) Balance between bonding and deposition during fused deposition modeling of polycarbonate and acrylonitrile-butadiene-styrene composites. Polym Compos 41(1):60–72
38. Zhou YG, Su B, Turng LS (2018) Mechanical properties, fiber orientation, and length distribution of glass fiber-reinforced polypropylene parts: influence of water-foaming technology. Polym Compos 39:4386–4399
39. Zhou YG, Su B, Turng LS (2017) Depositing-induced effects of isotactic polypropylene and polycarbonate composites during fused deposition modeling. Rapid Prototyp J 23:869–880
40. Zhou YG, Su B, Turng LS (2017) Influence of processing conditions on morphological structure and ductility of water-foamed injection molded PP/LDPE blended parts. Cell Polym 36:51–74
41. Zhou YG, Su B, Wu HH (2017) Effect of cold-drawn fibers on the self-reinforcement of the PP/LDPE composites. J Mater Eng Perform 26(8):4072–4082
42. Zhou YG, Su B, Turng LS (2016) Fabrication of super-ductile PP/LDPE blended parts with a chemical foaming agent. J Appl Polym Sci 133(42):44101
43. Zhang C, Zhai T, Turng LS, Dan Y, Morphological (2015) Mechanical, and crystallization behavior of polylactide/polycaprolactone blends compatibilized by L-lactide/caprolactone copolymer. Ind Eng Chem Res 54:9505–9511
44. Margolina E, Wu S (1988) Percolation model for brittle-tough transition in nylon/rubber blends. Polymer 29:2170–2173
45. Wu S (1985) Phase structure and adhesion in polymer blends: a criterion for rubber toughening. Polymer 26:1855–1863
46. Bartczak Z, Argon AS, Cohen RE, Weinberg M (1999) Toughness mechanism in semi-crystalline polymer blends: 1 high-density polyethylene toughened with rubber. Polymer 40:2331–2346
47. Kim GM, Michler GH (1998) Micromechanical deformation processes in toughened and particle-filled semicrystalline polymers: Part I characterization of deformation processes in dependence on phase morphology. Polymer 39:5689–5697
48. Kim GM, Michler GH (1998) Micromechanical deformation processes in toughened and particle-filled semicrystalline polymers: Part II model representation for micromechanical deformation processes. Polymer 39:5699–5703
49. Ren G, Sheng X, Qin Y, Chen X, Wang F (2014) Toughening of poly(propylene carbonate) using rubbery non-isocyanate polyurethane: transition from brittle to marginally tough. Polymer 55(21):5460–5468
50. Maragoni L, Talreja R (2019) Transverse crack formation in unidirectional plies predicted by means of a percolation concept. Compos Part A 117:317–323
51. Galeski A (2003) Strength and toughness of crystalline polymer systems. Prog Polym Sci 28:1643–1699
52. Rozanski A, Galeski A (2011) Controlling cavitation of semicrystalline polymers during tensile drawin. Macromolecules 44(18):7273–7287